

Far-infrared response of free charge carriers localized in semiconductor nanoparticles

Hynek Němec,^{1,2} Petr Kužel,¹ and Villy Sundström²

¹*Institute of Physics of the Academy of Sciences of the Czech Republic, Na Slovance 2, 182 21 Praha 8, Czech Republic*

²*Department of Chemical Physics, Lund University, Getingevägen 60, 222 41 Lund, Sweden*

(Received 21 November 2008; revised manuscript received 13 February 2009; published 12 March 2009)

A Monte Carlo method is employed to calculate the dynamical conductivity in the terahertz range of free charge carriers localized in semiconductor nanoparticles. The shape of the conductivity spectrum is essentially determined by the probability of carrier transition through interparticle boundaries and by the ratio of the nanoparticle size and carrier mean free path in the bulk. It is shown that the conductivity spectrum exhibits similar features as the classical extension of the Drude conductivity of electrons proposed by Smith [Phys. Rev. B **64**, 155106 (2001)]. We find and discuss the link of this model to the results of our simulations which suggests an interpretation of the phenomenological parameters of the Drude-Smith model.

DOI: 10.1103/PhysRevB.79.115309

PACS number(s): 78.47.jc, 72.20.-i

I. INTRODUCTION

The complex far-infrared conductivity of bulk crystalline semiconductors can be in a large majority of cases described by the classical Drude formula:¹

$$\sigma_D(\omega) = \frac{ne^2\tau_D}{m} \frac{1}{1 - i\omega\tau_D} \equiv ne\mu_D(\omega), \quad (1)$$

where e is the elementary charge, n is the density of conducting charge carriers (either due to doping or generated by photoexcitation), m is their effective mass, τ_D is their momentum relaxation time, and $\mu_D(\omega)$ is the frequency-dependent mobility.

Slightly improved Drude-type models were proposed to fit some particular conductivity data in the terahertz range.^{2,3} These models were aimed to account for a spectral distribution of carrier scattering times τ in analogy³ with the models previously developed to describe the distribution of relaxation times in dielectrics.⁴ All these conductivity models have two common features which are characteristic for an inductive-type response: (i) the real part of the conductivity decreases with frequency and (ii) the imaginary part is positive and peaks near the frequency corresponding to the mean carrier scattering rate ($\sim 1/\tau_D$).⁵

The far-infrared complex conductivity spectrum of many semiconductor or metallic nanoparticles fundamentally differs from this picture. Their response is essentially capacitive at low frequencies, i.e., it is characterized by an increasing real part of the conductivity and by a negative imaginary part.⁶⁻¹³

Time-resolved terahertz spectroscopy has become a spectroscopic tool *par excellence* to characterize dynamics and nanoscopic-scale transport of charge carriers in semiconductors (see Ref. 14 and references therein). Indeed, the optical pump-terahertz probe technique^{14,15} is a sensitive contact-free probe of the conductivity, which avoids complications arising from effects related to electrodes. Furthermore, the method is phase sensitive: both the real and imaginary parts of the conductivity are obtained independently from the raw experimental data. The complex spectra then can be confronted with the theoretical models providing an ultimate test of their validity.

Systems composed of nanoparticles are inhomogeneous and their macroscopic response is determined by two contributions which need to be addressed separately in our discussion: the contribution of local (depolarization) fields and that related to the localization and scattering of charge carriers.

Nanoparticles under investigation may be embedded in a matrix, i.e., samples may show some degree of porosity or contain voids of another dielectric. In such a case, local fields (on a length scale much smaller than the wavelength of the probing radiation) start to play a significant role and the experimentally observed effective conductivity response σ_{eff} may differ from the proper microscopic conductivity σ_{int} of closely packed nanoparticles. The response σ_{int} can be calculated from σ_{eff} by using appropriate effective-medium theory such as, e.g., the Maxwell-Garnett¹⁶ or Bruggeman¹⁷ model. Indeed, effective-medium theory was successfully applied to explain transient conductivity in relatively large ($\sim 10 \mu\text{m}$) silicon grains¹¹ and in nanoporous ($\sim 25 \text{ nm}$) TiO_2 .¹⁰ In these works, the mean free path of charge carrier was considerably shorter than the dimensions of the grains or nanoparticles; therefore the part of the response related to the interaction of carriers with the nanoparticle boundaries was negligible¹⁰ and the classical Drude model was able to describe the response of carriers: $\sigma_{\text{int}} = \sigma_D$. The presence and weight of the local-field contribution can be often checked by amplitude scaling of σ_{int} , e.g., by increasing the intensity of excitation. The effective response σ_{eff} then changes its spectral shape and even saturates when σ_{int} becomes sufficiently high.^{10,11}

In systems with a stronger charge localization, where the carrier mean free path is comparable to the characteristic dimension of the nanoparticles, the conductivity response becomes more complicated. A simple phenomenological extension of the Drude model proposed recently by Smith,¹⁸

$$\sigma_{\text{DS}}(\omega) = \frac{ne^2\tau_{\text{DS}}}{m} \frac{1}{1 - i\omega\tau_{\text{DS}}} \left(1 + \frac{c_1}{1 - i\omega\tau_{\text{DS}}} \right) \equiv ne\mu_{\text{DS}}(\omega), \quad (2)$$

was successfully applied to fit the conductivity in a large variety of systems.^{6-8,12,13} The parameter c_1 accounts for the anisotropy of scattering upon the first scattering event (c_1

$=0$ describes isotropic response which is proper to the Drude model; $c_1 < 0$ corresponds to a preferential backscattering of charge carriers). This parameter stays at the origin of the main criticism of the Drude-Smith model. The model assumes that anisotropic scattering occurs only upon the first scattering event, while all subsequent events are characterized by isotropic scattering.¹¹ However, no physical reasons were proposed to justify this assumption. In this context, the meaning of the parameter c_1 is not clear.

In this paper, we use a Monte Carlo method to calculate the far-infrared carrier mobility in systems composed of semiconducting nanoparticles. Only parameters with straightforward physical interpretation (nanoparticle dimensions, probability of the carrier transport among particles, carrier effective mass, temperature, and momentum scattering time) enter the simulation. It is assumed that the carrier scattering mechanisms inside the nanoparticles are the same as in the bulk material. The localized versus delocalized (bulklike) character of the far-infrared response is only determined by the interaction of carriers with the nanoparticle surface. We show that the calculated mobility spectra generally exhibit similar features as the Drude-Smith model [Eq. (2)]. We also demonstrate a relationship between the parameters of the Drude-Smith model and the microscopic properties. The developed theory is subsequently applied to interpret the transient terahertz response of ZnO and TiO₂ nanoparticles.

II. THEORETICAL MODEL

The model is based on Monte Carlo simulations of a thermal motion of charge carriers in a system of nanoparticles. The carriers move freely inside the nanoparticles and they are randomly scattered with mean time τ as in the bulk material. Each scattering event results in a randomization of their velocity vector \mathbf{v} according to the Maxwell-Boltzmann distribution. When the carrier reaches the nanoparticle boundary it may be scattered and the following three probabilities describe this interaction ($p_t + p_s + p_r = 1$):

(i) With a probability p_t the carrier continues its motion without interacting with the nanoparticle boundary.

(ii) The nanoparticle boundary isotropically scatters the carrier with probability p_s , i.e., the boundary acts as an additional scattering center. If this event occurs, then there are equal probabilities that the carrier enters another nanoparticle or that the carrier remains in the original one.

(iii) The carrier is reflected (scattered back) to the original nanoparticle with a probability p_r . Such a process arises due to energy barriers between the nanoparticles and it is at the origin of the carrier localization.

These events correspond to distinct physical processes but not necessarily to different carrier trajectories. In particular, the probability that the carrier remains in the original nanoparticle is $p_t + p_s/2$, while the probability that it enters another one is $p_t + p_s/2$. The latter expression can be understood as a permeability of the nanoparticle boundary.

The mobility of carriers is then calculated using the Kubo formula,¹⁹

$$\mu_{ij}(\omega) = \frac{e_0}{k_B T} \int_0^\infty \langle v_i(0)v_j(t) \rangle e^{i\omega t} dt, \quad (3)$$

where k_B is the Boltzmann constant. The averaging takes place over a canonical ensemble of carriers represented by a temperature T . For the sake of simplicity, we consider spherical nanoparticles with diameter d . Such a system is macroscopically isotropic; therefore it is characterized by a single mobility, which is equal to the diagonal elements of the mobility tensor μ_{ii} . The conductivity of the sample is then equal to $\sigma = en\mu_{ii}$.

Important parameters entering the simulations are the thermal velocity,

$$v_{\text{therm}} = \sqrt{\frac{3k_B T}{m}}, \quad (4)$$

the bulk carrier momentum scattering time τ , the carrier mean free path $l_{\text{free}} = v_{\text{therm}}\tau$, and the ratio α of the carrier mean free path and the nanoparticle diameter ($\alpha = d/l_{\text{free}}$). Many of these input parameters are mutually connected and, by analyzing Eq. (3), one can find specific scaling rules which are important for subsequent discussion and for the reduction in the number of representative simulations (in the following we do not consider the carrier mass m as a variable parameter).

(i) We scale both d and l_{free} by a factor γ and we formally assume that the scaling of the mean free path is connected to the appropriate change in the thermal velocity [or equivalently, to the change in the temperature through Eq. (4)]. These conditions imply that the scattering rates both in the bulk and at the nanoparticle boundaries are not modified. It follows that the integrand of Eq. (3) is proportional to the temperature and the resulting mobility does not change. In other words, scaling the thermal velocity (or temperature) is equivalent to an appropriate scaling of the system dimensions.

(ii) We scale d and l_{free} by a factor γ while keeping the thermal velocity constant. In this case both bulk and surface scattering times are scaled by the same factor γ , which implies the time and frequency scalings in Eq. (3): $t \rightarrow \gamma t$, $\omega \rightarrow \omega/\gamma$, and finally, $\mu(\omega) \rightarrow \gamma\mu(\omega/\gamma)$.

These scaling rules are quite apparent, and we have also verified their validity by numerical simulations. From this discussion it follows that the shape of the spectrum is determined only by the parameters α , p_r , and p_s , while the remaining parameters only determine the pertinent scales (length, time, frequency, and mobility amplitude).

Examples of the calculated complex mobility spectra for isolated nanoparticles ($p_r = 1$) are shown in Fig. 1. The mobility approaches zero at sufficiently low frequencies for finite α since the localization cancels the long-range transport. The real part of the mobility spectrum shows a peak, therefore the imaginary part must become negative in a certain spectral interval in order to satisfy the Kramers-Kronig relations (analogously to the conductivity spectrum of bound charges¹⁴). It should be noted that these characteristics are valid for any finite value of α , but they are not clearly visible in the plots for high values of α due to the restricted time

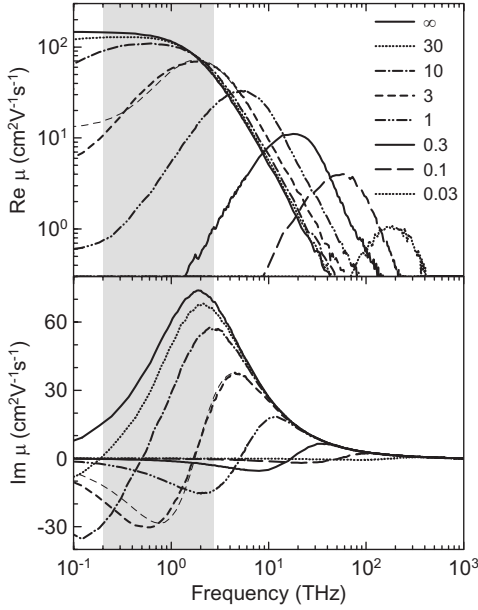


FIG. 1. Mobility spectra calculated using the Monte Carlo method for $p_r=1$ and $p_s=p_t=0$ for various values of α . The other parameters of the simulation were $l_{\text{free}}=10$ nm, $v_{\text{therm}}=1.17 \times 10^5$ m s $^{-1}$ ($T=300$ K), and $\tau=85.6$ fs. The thin dashed line illustrates a Drude-Smith fit over the entire plotted spectral range for $\alpha=3$ which yields parameters $\tau_{\text{DS}}=83$ fs and $c_1=-0.912$ (the line is not shown above 5 THz as it is indistinguishable from the line corresponding to the mobility calculated by the Monte Carlo method).

window in the numerical simulations [the upper integration limit in Eq. (3) is finite]. The peak in the real part decreases in amplitude and its frequency f_0 shifts to higher frequencies upon decreasing α (enhanced localization). The position of the peak is closely related to the ballistic round-trip time of carriers in the sphere $\tau_{\text{rt}}=2d/v_{\text{therm}}$: we find that a relation $f_0 \approx 0.9/\tau_{\text{rt}}$ is quite well satisfied for $\alpha \lesssim 30$. With increasing α more scattering events occur during the round trip and for $\alpha \gtrsim 30$ the resonance frequency is no longer well defined in the spectra. The decrease in the conductivity amplitude with decreasing α is related to the fact that the effective carrier scattering is enhanced by frequent reflections at the nanoparticle surface.

The situation is only slightly different for lower values of p_r . Examples of spectra for several values of α and $p_r=p_s=0.5$ ($p_t=0$) are shown in Fig. 2. The most remarkable difference consists in a nonvanishing real part of the mobility at zero frequency, which is caused by the fact that the charges may pass from one nanoparticle to another and the long-distance transport is thus enabled. Other features (peak in the real part of the mobility shifting with α , negative imaginary part of the mobility at low frequencies) are similar to the preceding case.

For $p_r=0$ the carrier localization is lost and the nanoparticle boundaries contribute merely to the isotropic scattering process ($p_s=1$) or they have completely no influence ($p_t=1$). The mobility is then described by the Drude formula; in the former case, the effective carrier scattering time is shortened compared to the bulk material. Such a type of behavior was observed in CdSe nanoparticles.²⁰

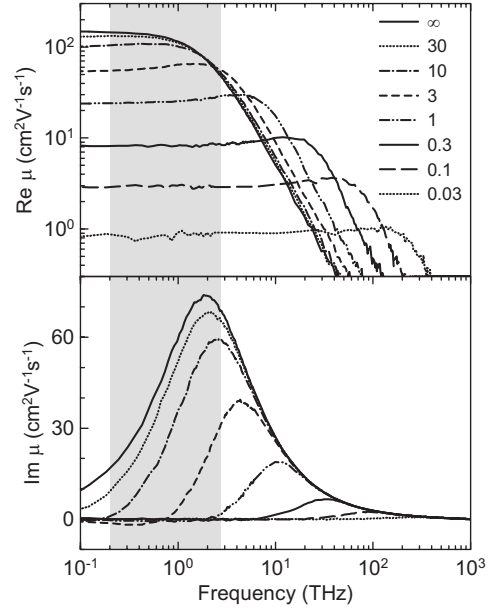


FIG. 2. Mobility spectra calculated using the Monte Carlo method for $p_r=p_s=0.5$ ($p_t=0$) and for various α . The other parameters of the simulation were $l_{\text{free}}=10$ nm, $v_{\text{therm}}=1.17 \times 10^5$ m s $^{-1}$, and $\tau=85.6$ fs.

Analogous calculations and discussion can be carried out for any other value of p_r . Since the dependence on p_r is smooth, the analysis of the results for $p_r=0, 0.5, 1$ is sufficient to obtain a clear picture for any p_r and α . Briefly summarized, there is a smooth transition from a bulklike free-carrier response toward a localized response with increasing p_r and decreasing α .

III. DISCUSSION

In practice only restricted spectral intervals can be investigated experimentally: here we consider 0.5–2.8 THz for illustration (marked in gray in Figs. 1 and 2) as this range is usually accessible in standard optical pump-terahertz probe experiments. In this range the mobility can be well fitted using the Drude-Smith model for any combination of parameters we studied. We also confirm that, even if the maximum of the mobility peak occurs above the spectral range considered for the fits, the position of the peak as determined by the Drude-Smith fit matches the one found in the simulations: $f_{0,\text{DS}} \approx f_0$. In addition, for $p_r=1$, where the full width at half maximum (FWHM) Δf of the conductivity peak can be well defined, we find approximately $\Delta f \approx \Delta f_{\text{DS}}$. However, we stress that the Drude-Smith fit over a broad spectrum, which encompasses the whole range of the conductivity dispersion is poor and shows systematic deviations from the simulated data: in particular, $\text{Re } \mu$ approaches a wrong value for $f \rightarrow 0$. This is illustrated by the thin dashed line in Fig. 1.

The fit parameter values obtained when the reduced spectral range was fitted are summarized in Fig. 3. For $\alpha \gtrsim 30$ the best fit is obtained with a Drude spectrum ($c_1=0$) where $\tau_{\text{DS}}=\tau$. A clear departure from the Drude model is observed for $\alpha \lesssim 30$. The Drude-Smith parameters c_1 and τ_{DS} vary

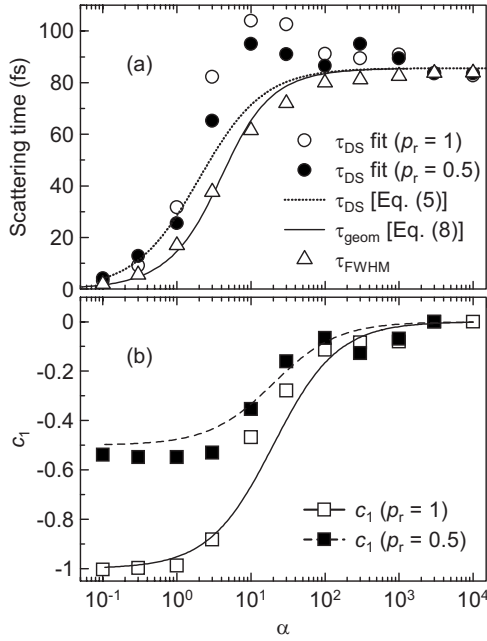


FIG. 3. Parameters obtained by fitting the mobility spectra from Figs. 1 and 2 using the Drude-Smith model in the spectral interval from 0.5 to 2.8 THz. (a) Closed circles: $\rho_r=1$, opened circles: $\rho_r=\rho_s=0.5$. The lines indicate the Matthiessen's rule [Eq. (5)] and the geometrical approximation of the scattering time [Eq. (8)]. The triangles express $\tau_{FWHM}=1/(2\pi\Delta f)$ for $\rho_r=1$, where Δf is the FWHM of the simulated mobility peak. (b) Symbols: parameters c_1 from the Drude-Smith fit, lines: approximation by Eq. (6).

with α . With decreasing α the parameter c_1 becomes negative and τ_{DS} decreases as intuitively expected. For $\alpha \lesssim 1$ the spectrum resembles the Drude-Smith model with $c_1 \sim -\rho_r$, but the value of τ_{DS} is much smaller than τ and it is essentially determined by the mean time between collisions at the surfaces.

For practical purposes, it may be convenient to express the results of Monte Carlo simulations in terms of parameters of a simple analytical model. We find that τ_{DS} follows well the Matthiessen's rule,

$$\frac{1}{\tau_{DS}} = \frac{1}{\tau} + \frac{1}{\tau_\alpha}. \quad (5)$$

We assume that the mean scattering time τ_α due to the nanoparticle boundaries is proportional to d/v_{therm} (i.e., to τ_r). A good match with values of τ_{DS} obtained by fitting the Monte Carlo results is achieved with $\tau_\alpha \approx d/(2v_{\text{therm}}) = \tau\alpha/2$ (dotted line in Fig. 3). It is interesting to note that a similar sharp step is found in the α dependence of c_1 :

$$c_1 = -\frac{\rho_r}{1 + \tau'_\alpha/\tau}, \quad (6)$$

but it occurs at about ten times higher values of α as compared to τ_{DS} ($\tau'_\alpha \approx \tau_\alpha/10$). It should be noted that Eqs. (5) and (6) were obtained for a specific fitting range. It is likely that the particular numerical coefficients will vary upon choosing a different spectral range for fitting the Drude-Smith model. Also the values of numerical coefficients are

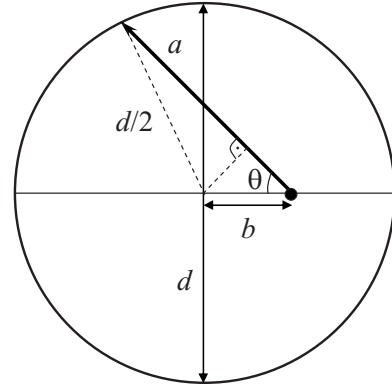


FIG. 4. Scheme for the geometrical model of charge-carrier scattering in a spherical nanoparticle.

expected to change if a nonspherical shape of nanoparticles is considered.

To obtain a deeper insight into the relation between the Drude-Smith model and the Monte Carlo simulations, we developed a simple geometrical model allowing us to estimate the mean scattering time τ_{geom} of the localized carriers. The geometrical parameters for a spherical nanoparticle are shown in Fig. 4. We consider that the charge is at the distance b from the nanoparticle center and that it moves in some random direction described by the angle θ . It may be scattered either in the bulk (this is described by an exponential law with a time constant τ) or (at the latest) at the nanoparticle boundary after passing the distance a which depends on the direction of its motion. After some trigonometrical considerations one easily finds $a = b \cos \theta + \sqrt{(d/2)^2 - b^2 \sin^2 \theta}$. The mean scattering time for such a charge is equal to

$$\bar{\tau} = \frac{\int_0^{a/v_{\text{therm}}} t p(t) dt}{\int_0^{a/v_{\text{therm}}} p(t) dt} = \tau \left[1 - \frac{a}{l_{\text{free}}} \frac{1}{\exp(a/l_{\text{free}}) - 1} \right], \quad (7)$$

where $p(t) = \exp(-t/\tau)$ is proportional to the probability density that the carrier is scattered at time t . We have to average over all possible directions of carrier motion and over all possible starting points determined by b . To calculate this value we assume that all the initial conditions are equiprobable (this assumption is not completely justified, nevertheless within this approximation a good match with the Drude-Smith model is obtained). The geometrical approximation of the scattering time τ_{geom} reads as

$$\tau_{\text{geom}} = \int_0^{d/2} \frac{4\pi b^2 db}{(4/3)\pi(d/2)^3} \int_0^\pi \frac{\sin \theta d\theta}{2} \bar{\tau}(\theta, b). \quad (8)$$

After a straightforward substitution we find that the shape of τ_{geom} depends only on α ; this dependence is shown in Fig. 3. We find that τ_{geom} is an excellent estimate of the FWHM of the mobility peak Δf : $\tau_{\text{geom}} \approx \tau_{FWHM} \equiv 1/(2\pi\Delta f)$ (Fig. 3).

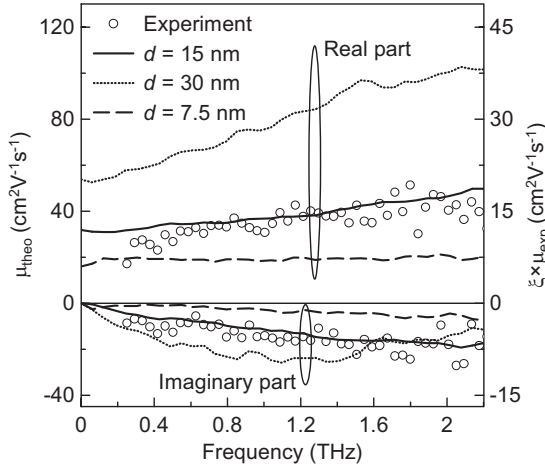


FIG. 5. Spectra of carrier mobility in ZnO nanoparticles (pump-probe delay: 20 ps, excitation density: ~ 7 carriers per nanoparticle). Points: experimental results (right axis), lines: results of the Monte Carlo modeling ($p_r=0.8$; left axis) for $d=30$ nm (dotted line), 15 nm (solid line), and 7.5 nm (dashed line).

In the Drude-Smith model for $c_1=-1$, the mobility maximum occurs at $f_{0,DS}=1/(2\pi\tau_{DS})$ and the full width at half maximum of the peak equals $\Delta f_{DS}=1/(\pi\tau_{DS})$. Thus the phenomenological parameter τ_{DS} characterizes both the effective restoring force and the scattering time of carriers. In contrast, in the Drude limit (i.e., $c_1=0$) τ_{DS} keeps only the meaning of the carrier scattering time with $\Delta f_{DS}=1/(2\pi\tau_{DS})$. Let us consider a set of samples consisting of nanoparticles with identical properties but with a variable diameter. For $\alpha \lesssim 1$ we obtain $c_1=-p_r$; in this regime the dynamics is governed by τ_{geom} which has the meaning of the scattering time (dissipative interaction). In particular, for $p_r=1$, τ_{geom} is also connected to the Drude-Smith restoring force: $\tau_{DS} \approx 2\tau_{geom}$. In the transition range $3 \lesssim \alpha \lesssim 100$ the Drude-Smith parameter c_1 significantly varies for $p_r > 0$, which means that the conductivity peak shifts to zero frequency and at the same time the physical nature of τ_{DS} changes and it becomes purely dissipative ($\tau_{DS} \rightarrow \tau_{geom}$). For large nanoparticles ($\alpha \gtrsim 100$) the Drude-type regime is restored with $\tau_{geom}=\tau$.

From our discussion we can draw some implications for the interpretation of results obtained in a limited spectral interval. We have observed that it is possible to fit the simulated data by the phenomenological Drude-Smith model in the low-frequency part and extrapolate the fit to find the position of the conductivity peak. The value of τ_{DS} is closely connected to the degree of localization of carriers inside nanoparticles; the change in the carrier scattering regime occurs at $d/l_{free} \approx 1-5$ following Fig. 3. This behavior is reproduced by a simple geometrical model of carrier scattering inside a nanoparticle. For $\alpha \gtrsim 30$ a lack of low-frequency experimental data may lead to a quantitatively wrong conclusion that there is a long-range transport undisturbed by particle boundaries. For lower values of α , the signatures of localization start to appear in the THz spectra, but it is still impossible, e.g., to infer quantitatively on the degree of permeability of the nanoparticle boundaries. The most correct picture is obtained for sufficiently low values of α ($\alpha \lesssim 1$) for which $c_1 \approx -p_r$ and the scattering time is driven by col-

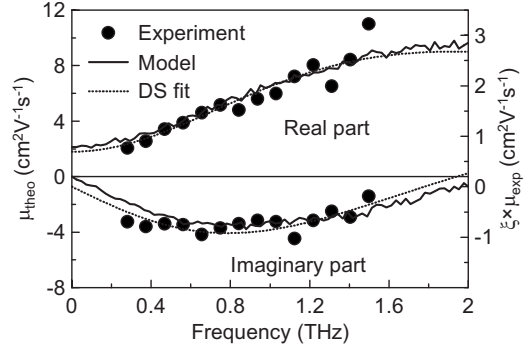


FIG. 6. Spectra of carrier mobility in TiO₂ nanoparticles. Points: experimental results (right axis), solid lines: results of the Monte Carlo modeling ($p_r=0.9$, left axis). A Drude-Smith fit ($\tau_{DS}=77$ fs and $c_1=-0.87$) of the experimental data is illustrated by the dotted line.

lisions of charges with the nanoparticle boundary.

Real samples are characterized by a distribution of nanoparticle sizes. The photoconductivity response then will be inhomogeneously broadened. Larger grains will contribute more to the averaged response function as they exhibit a higher amplitude of mobility (Figs. 1 and 2).

IV. RESPONSE OF ZnO AND TiO₂ NANOPARTICLES

In this paper we show some experimental results we have obtained by time-resolved THz spectroscopy on ZnO and TiO₂ nanoparticle systems. These selected data are not exhaustive and they are presented here in order to illustrate our simulations. Therefore we do not discuss here experimental details; comprehensive papers on the investigation of these nanoparticle systems will be published elsewhere.

The films of ZnO nanoparticles were prepared by a sol-gel technique²¹ that produced mesoporous films 600 nm thick. These consist of nanoparticles with an average diameter of ~ 15 nm. Their transient terahertz conductivity was measured in a usual setup for optical pump-terahertz probe experiments that we described, e.g., in Ref. 22. The optical excitation of samples was accomplished by the third harmonic of a femtosecond Ti:sapphire laser (≈ 266 nm) in order to generate free carriers through an interband transition in ZnO. The size of the excitation beam (4.5 mm full width at half maximum) was larger than the THz beam size ($\lesssim 3$ mm) and the sample was placed on a 3 mm diameter metallic aperture, so possible artifacts due to finite pump-beam size should be avoided. Formulas from Ref. 23 (which apply in the small signal limit) were used for the retrieval of the time-resolved conductivity from transient transmittance spectra.

The studied samples were mixtures of ZnO nanoparticles forming a percolated network filled with air voids. The transient conductivity obtained from the experiments then corresponded to the effective conductivity of the studied films. We applied the Maxwell-Garnett theory¹⁶ to relate the effective properties of the film with the intrinsic properties of the nanoparticles. We considered the sample as a ZnO matrix filled with air voids with volume fraction 35% which corre-

sponds to the filling factor of voids in an array of closely packed spheres with a given diameter. Taking into account the permittivity of bulk ZnO ($\epsilon_{\text{ZnO}}=7.8$)²⁴ we found that the (measured) effective transient conductivity of the film scales linearly with the (sought) transient conductivity of nanoparticles, the proportionality constant of 0.55 being practically independent of the frequency and conductivity amplitude. Note that the directly accessible quantity in the experiment is $\xi\mu$, where ξ is the quantum yield of conversion of pump photons into mobile charge carriers interacting with THz radiation. This value is quite difficult to determine accurately due to the large absorption of the film. A part of the excitation pulse energy is reflected and another part is scattered by the film. Also a part of the excitation radiation can be absorbed at nanoparticle boundaries generating immobile (trapped) carriers. The charge-carrier mobility in the ZnO nanoparticles deduced from the experimental data is shown in Fig. 5 for the excitation fluence of 8×10^{13} photons/cm². The lifetime of the transient signal is ~ 400 ps. The same shape of spectra is obtained for a broad range of pump intensities (corresponding to 0.5–20 photoexcited carriers per nanoparticle).

In the Monte Carlo simulation of the mobility [Eq. (3)], we considered electrons with $m=0.24m_e$ and $\tau=27$ fs,²⁵ hence $l_{\text{free}}=6.4$ nm and $\alpha=2.3$. In order to match the experimental mobility with the simulations the quantum yield ξ should be equal to 0.4 and $p_r=0.8$. Note that ξ and p_r are the only adjustable parameters: values of all other parameters are known. The important point is the close match in the spectral shapes of the intrinsic mobility for $d=15$ nm, which corresponds to the nominal size of the nanoparticles. Spectral shapes calculated with different values of d significantly differ from the measured spectrum (Fig. 5).

Similar experiments were performed with samples consisting of TiO₂ nanoparticles with average diameter of 9 nm (Ti-nanoxide HT paste from Solaronix SA). The $\xi\mu$ product obtained with the pump wavelength of 300 nm and excitation fluence of 1×10^{14} photons/cm² is plotted in Fig. 6. The spectrum agrees well with the mobility calculated using the Monte Carlo method with the following parameters: $p_r=0.9$, $m \approx 6m_e$ (Ref. 26), and $\tau=100$ fs (measured in our laboratory with a TiO₂ single crystal), i.e., $l_{\text{free}}=4.8$ nm and

$\alpha=1.9$. The amplitudes of mobilities match for $\xi=0.3$.

From the simulations, we can conclude that the long-range transport of electrons in the investigated ZnO and TiO₂ nanoparticles is largely inhibited by the localization; the dc mobility is respectively decreased by a factor of ~ 5 and ~ 10 as compared to the bulk materials. This implies that the nanoparticles form densely packed structures. The observation is related to the reflection probabilities $p_r=0.8$ for ZnO and $p_r=0.9$ for TiO₂. The rather small values of ξ may be related to uncertainties in the determination of the excitation density but they may also indicate that a part of the electrons is generated in initially immobile states.

V. CONCLUSIONS

We have developed a framework for quantitative understanding the far-infrared response of charge carriers localized in nanoparticles. The shape of the spectrum is fully determined by the ratio of the nanoparticle size and carrier mean free path and by the permeability of the nanoparticle boundaries (or the probability of carrier reflection from the nanoparticle surface); the pertinent frequency scale and mobility amplitude is given by the nanoparticle size. The mobility spectrum in a broad spectral range does not generally follow the Drude-Smith model. Nevertheless, Eqs. (5) and (6) constitute the link relating the parameters of the Drude-Smith fit in a narrow spectral region and the microscopic parameters p_r and τ . The proposed model was also used for the interpretation of electron mobility measured by time-resolved terahertz spectroscopy in ZnO and TiO₂ nanoparticles.

ACKNOWLEDGMENTS

The authors thank Elena Galoppini and Olena Taratula of Rutgers University for providing the ZnO nanoparticle films and Ping Zuo of Lund University for the preparation of the TiO₂ films. The financial support from the Ministry of Education (Project No. LC512) and Czech Science Foundation (Project No. 202/09/P099) is acknowledged. The work at Lund University was supported by grants from the Swedish Energy Agency (STEM) and Knut and Alice Wallenberg Foundation.

¹D. Grischkowsky, S. Keiding, M. van Exter, and C. Fattinger, *J. Opt. Soc. Am. B* **7**, 2006 (1990).

²T.-I. Jeon and D. Grischkowsky, *Phys. Rev. Lett.* **78**, 1106 (1997).

³M. C. Beard, G. M. Turner, and C. A. Schmuttenmaer, *Phys. Rev. B* **62**, 15764 (2000).

⁴A. K. Jonscher, *Dielectric Relaxation in Solids* (Chelsea, New York, 1983).

⁵Note that the positive imaginary conductivity corresponds to the negative contribution of free carriers to the dielectric permittivity.

⁶J. B. Baxter and C. A. Schmuttenmaer, *J. Phys. Chem. B* **110**, 25229 (2006).

⁷M. C. Beard, G. M. Turner, J. E. Murphy, O. I. Micic, M. C. Hanna, A. J. Nozik, and C. A. Schmuttenmaer, *Nano Lett.* **3**, 1695 (2003).

⁸D. G. Cooke, A. N. MacDonald, A. Hryciw, J. Wang, Q. Li, A. Meldrum, and F. A. Hegmann, *Phys. Rev. B* **73**, 193311 (2006).

⁹L. Fekete, H. Němec, F. Kadlec, P. Kužel, J. Stuchlík, A. Fejfar, and J. Kočka, *J. Non-Cryst. Solids* **352**, 2846 (2006).

¹⁰E. Hendry, M. Koeberg, B. O'Regan, and M. Bonn, *Nano Lett.* **6**, 755 (2006).

¹¹H.-K. Nienhuys and V. Sundström, *Appl. Phys. Lett.* **87**, 012101 (2005).

¹²G. M. Turner, M. C. Beard, and C. A. Schmuttenmaer, *J. Phys. Chem. B* **106**, 11716 (2002).

- ¹³M. Walther, D. G. Cooke, C. Sherstan, M. Hajar, M. R. Freeman, and F. A. Hegmann, *Phys. Rev. B* **76**, 125408 (2007).
- ¹⁴F. A. Hegmann, O. Ostroverkhova, and D. G. Cooke, *Photophysics of Molecular Materials* (Wiley-VCH Verlag GmbH & Co. KGaA, Weinheim, 2006), Chap. 7, pp. 367–428.
- ¹⁵C. A. Schmuttenmaer, *Chem. Rev.* **104**, 1759 (2004).
- ¹⁶J. C. M. Garnett, *Philos. Trans. R. Soc. London, Ser. A* **203**, 385 (1904).
- ¹⁷D. A. G. Bruggeman, *Ann. Phys.* **416**, 636 (1935).
- ¹⁸N. V. Smith, *Phys. Rev. B* **64**, 155106 (2001).
- ¹⁹R. Kubo, *J. Phys. Soc. Jpn.* **12**, 570 (1957).
- ²⁰M. C. Beard, G. M. Turner, and C. A. Schmuttenmaer, *Nano Lett.* **2**, 983 (2002).
- ²¹O. Taratula, E. Galoppini, D. Wang, D. Chu, Z. Zhang, H. Chen, G. Saraf, and Y. Lu, *J. Phys. Chem. B* **110**, 6506 (2006).
- ²²H. Němec, F. Kadlec, C. Kadlec, P. Kužel, and P. Jungwirth, *J. Chem. Phys.* **122**, 104504 (2005).
- ²³P. Kužel, F. Kadlec, and H. Němec, *J. Chem. Phys.* **127**, 024506 (2007).
- ²⁴J. Han, Z. Zhu, S. Ray, A. K. Azad, W. Zhang, M. He, S. Li, and Y. Zhao, *Appl. Phys. Lett.* **89**, 031107 (2006).
- ²⁵S. J. Pearton, D. P. Norton, K. Ip, Y. W. Heo, and T. Steiner, *Prog. Mater. Sci.* **50**, 293 (2005).
- ²⁶E. Hendry, F. Wang, J. Shan, T. F. Heinz, and M. Bonn, *Phys. Rev. B* **69**, 081101(R) (2004).